Journal of Computational Physics 439 (2021) 110402

Contents lists available at ScienceDirect

Journal of Computational Physics

www.elsevier.com/locate/jcp

Three dimensional high-order gas-kinetic scheme for supersonic isotropic turbulence II: Coarse-graining analysis of compressible K_{sgs} budget

Guiyu Cao [a,b], Liang Pan [c], Kun Xu [b,d,*]

[a] Academy for Advanced Interdisciplinary Studies, Southern University of Science and Technology, Shenzhen, China
[b] Department of Mathematics, Hong Kong University of Science and Technology, Clear Water Bay, Kowloon, Hong Kong
[c] Laboratory of Mathematics and Complex Systems, School of Mathematical Sciences, Beijing Normal University, Beijing, China
[d] Shenzhen Research Institute, Hong Kong University of Science and Technology, Shenzhen, China

ARTICLE INFO

Article history:
Available online 5 May 2021

Keywords:
High-order gas-kinetic scheme
Supersonic isotropic turbulence
Compressible K_{sgs} transport equation
Coarse-graining budget analysis

ABSTRACT

The direct numerical simulation (DNS) of compressible isotropic turbulence up to the supersonic regime with $Ma_t = 1.2$ has been investigated by the high-order gas-kinetic scheme (HGKS) (Cao et al. (2019) [8]). In this study, the DNS on a much higher initial turbulent Mach number up to $Ma_t = 2.0$ is performed by HGKS, which confirms the super robustness of HGKS. The coarse-graining analysis of subgrid-scale (SGS) turbulent kinetic energy K_{sgs} budget is fully analyzed for constructing one-equation SGS model in the compressible large eddy simulation (LES). The exact compressible SGS turbulent kinetic energy K_{sgs} transport equation is derived with density weighted filtering process. Based on the compressible K_{sgs} transport equation, the coarse-graining processes are implemented on three sets of unresolved grids with the Box filter. The coarse-graining analysis of compressible K_{sgs} budgets shows that all unresolved source terms are dominant in the current system. Especially, the magnitude of SGS pressure-dilation term is on the order of SGS solenoidal dissipation term within the initial acoustic time scale. Therefore, the SGS pressure-dilation term cannot be neglected as that in the previous work. The delicate coarse-graining analysis of SGS diffusion terms in compressible K_{sgs} equation also confirms that both the fluctuation velocity triple correlation term and the pressure-velocity correlation term are dominant terms. The current analysis provides an indication on the order of magnitude of all SGS terms in compressible K_{sgs} budget, which provides a solid basis for compressible LES modeling of high Mach number turbulent flow.

1. Introduction

The supersonic turbulence plays a key role in a wide range of natural phenomena and engineering applications, such as interstellar turbulence, hypersonic spacecraft reentry, and nuclear fusion power reactors [1,2]. Compared with incompressible turbulence, highly compressible turbulent flows are more complex due to the nonlinear coupling of velocity, density and pressure fields [3]. To elucidate the effects of compressibility in the compressible turbulence, the compressible isotropic turbulence is regarded as one of cornerstones [4–6]. However, for the compressible isotropic turbulence in supersonic regime

* Corresponding author: Department of Mathematics, Hong Kong University of Science and Technology, Clear Water Bay, Kowloon, Hong Kong.
E-mail addresses: caogy@sustech.edu.cn (G. Cao), panliang@bnu.edu.cn (L. Pan), makxu@ust.hk (K. Xu).

https://doi.org/10.1016/j.jcp.2021.110402
0021-9991/

($Ma_t \geq 0.8$), the strong random shocklets and high spatial-temporal gradients pose great difficulties for both theoretical analyses and numerical studies in comparison with the flow in other regimes [5,7,8]. Currently, the study of supersonic regime is much less known and reported, and very few numerical experiments are available [9,8,10]. For compressible turbulence modeling, the large eddy simulation (LES) for high Mach number turbulent flows is rarely reported.

One-equation subgrid-scale (SGS) models have been extensively used in incompressible LES [11–14]. Since the incorporation of history and non-local effects through transport equation related to the residual motions, the one-equation SGS models have shown better performance in the prediction of turbulent flow. Meanwhile, compared with the abundant research on compressibility correction for the turbulent kinetic energy equation in the Reynolds averaged Navier-Stokes (RANS) simulation [15–21], there only exists limited number of research work on compressible one-equation SGS models for the compressible LES [22–25]. With the rapid increasing of computational power, it is well known that the LES gradually becomes the workhorse for high-fidelity turbulence simulation from the smooth turbulent flow to the supersonic one [26]. However, as far as we know, the compressible LES models are less reported, where the algebraic eddy viscosity model can be hardly incorporated with the compressible effect systematically [27,28]. In the modeling of the compressible effect, it is natural to extend the one-equation SGS model to high turbulent Mach number flow. For compressible one-equation SGS model, an important issue that has not been resolved in the earlier studies is how to distinguish the dominant terms and negligible ones. Very few coarse-graining analysis of compressible turbulence has been carried out in LES [29–31], where most of them are limited to the subsonic turbulent Mach number ($Ma_t \leq 0.8$). The priori tests using direct numerical simulation (DNS) data for the calculation of a mixing layer up to Mach number 0.6 [29,30], and the DNS for the homogeneous isotropic turbulence up to $Ma_t = 0.52$, were filtered for the computation of the unclosed terms in the momentum, internal energy, and total energy equations [31]. It is emphasized that the unresolved dilational dissipation rate and the unresolved pressure-dilation term are important to the compressible LES. For the forced supersonic isotropic turbulence ($Ma_t \approx 1.0$), the filtered result of turbulent kinetic energy transfer on unresolved grids has been well studied [32]. With the objective of constructing one-equation SGS model for a much higher turbulent Mach number flow, i.e., $Ma_t \geq 1.0$, the detailed analysis of coarse-grained turbulent kinetic energy budget K_{sgs} is much required in the modeling.

In the past decades, the gas-kinetic scheme (GKS) based on the Bhatnagar-Gross-Krook (BGK) model [33,34] has been developed systematically for the computations from low speed flow to hypersonic one [35–37]. Based on the time-dependent flux solver, including generalized Riemann problem solver and gas-kinetic scheme [38,39], a reliable framework was provided for developing the GKS into fourth-order and even higher-order accuracy [40–42]. More importantly, these high-order schemes are as robust as the second-order one and work perfectly from the subsonic to the hypersonic viscous heat conducting flows. In recent years, the GKS has been applied in high-Reynolds number turbulent flow [43,44]. Considering the space-time coupled evolution and robustness, the high-order gas-kinetic scheme (HGKS) has been used as a DNS tool for the compressible isotropic turbulence up to supersonic regime $Ma_t = 1.2$ [8]. This study confirms that the HGKS provides a valid tool for the simulation of supersonic isotropic turbulence, and the criterion for DNS solution is also determined. Following the first part [8], in order to construct one-equation SGS model for compressible LES, the coarse-graining analysis on supersonic isotropic turbulence is studied in this paper. The DNS on a much higher initial turbulent Mach number ($Ma_t = 2.0$) is conducted, and the exact compressible turbulent kinetic energy K_{sgs} transport equation has been derived through a density weighted filtering process. Based on the high-fidelity DNS data, the coarse-graining processes are implemented in physical space with a Box filter. The compressible K_{sgs} budget is fully analyzed and the dominant terms are categorized. Current coarse-graining analysis provides a solid basis for the compressible LES modeling in the high Mach number turbulent flow.

This paper is organized as follows. In Section 2, the DNS results of supersonic isotropic turbulence by HGKS are presented. Section 3 constructs the transport equation for the compressible SGS turbulent kinetic energy K_{sgs} through the coarse-graining analysis on the solutions of different grids. Conclusion is drawn in the final section.

2. DNS of supersonic isotropic turbulence

The decaying compressible isotropic turbulence is regarded as one of fundamental benchmarks in the study the compressible effect [3,5,45]. The domain of numerical simulation is a cube box defined as $[-\pi, \pi] \times [-\pi, \pi] \times [-\pi, \pi]$, with periodic boundary conditions in all three Cartesian directions for all the flow variables. Evolution of this artificial system is determined by initial thermodynamic quantities and two dimensionless parameters, i.e., the initial Taylor microscale Reynolds number $Re_\lambda = \langle \rho \rangle U_{rms} \lambda / \langle \mu \rangle$ and the initial turbulent Mach number $Ma_t = \sqrt{3} U_{rms} / \langle c_s \rangle$, where $\langle \cdot \rangle$ is the ensemble over the whole computational domain, ρ is the density, λ is the Taylor microscale, μ is the initial dynamic viscosity, c_s is the sound speed, and U_{rms} is the root mean square of initial turbulent velocity component $U_{rms} = \langle \boldsymbol{U} \cdot \boldsymbol{U} / 3 \rangle^{1/2}$. A three-dimensional solenoidal random initial velocity field $\boldsymbol{U}$ can be generated by a specified spectrum [46], which is given by

$$E(\kappa) = A_0 \kappa^4 \exp(-2\kappa^2/\kappa_0^2), \tag{1}$$

where A_0 is a constant to get a specified initial kinetic energy, κ is the wave number, κ_0 is the wave number at which the spectrum peaks. In this paper, the fixed $A_0 = 0.00013$ and $\kappa_0 = 8$ in Eq. (1) are chosen for all cases.

Initial set-up plays an important role in compressible isotropic turbulence simulation [45], especially in the starting fast transient period during which the divergence of the velocity increases rapidly and the negative temperature or pressure

Table 1
Parameters for supersonic isotropic turbulence of test R_1 and test R_2, where $\kappa_{max} = \sqrt{2}\kappa_0 N/3$ is maximum resolved wave number [48], N is the number of grid points in each Cartesian direction and Δt_{ini} represents the time step for the initial step.

Test	Grid size	Ma_t	Re_λ	$\kappa_{max}\eta_0$	$\Delta t_{ini}/\tau_{to}$
R_1	384^3	2.0	72	2.71	2.00/1000
R_2	512^3	2.0	120	2.80	3.40/1000

often appears. In the computation, the initial pressure p_0, density ρ_0 and temperature T_0 are set as constants. In this way, the initial Taylor microscale Reynolds number Re_λ and the initial turbulent Mach number Ma_t can be determined by

$$\begin{aligned} Re_\lambda &= \frac{(2\pi)^{1/4}}{4}\frac{\rho_0}{\mu_0}\sqrt{2A_0}\kappa_0^{3/2}, \\ Ma_t &= \frac{\sqrt{3}}{\sqrt{\gamma RT_0}}U_{rms}, \end{aligned}$$

where the initial density $\rho_0 = 1$, μ_0, T_0 are determined by Re_λ and Ma_t, and $\gamma = 1.4$ is the specific heat ratio. In the simulation, the dynamic viscosity coefficient is given by $\mu = \mu_0(T/T_0)^{0.76}$. The equation of state is adopted as the idea gas $p = \rho RT$, R is the gas constant, and the Prandtl number is $Pr = 1$. With current initial set-up, the initial ensemble turbulent kinetic energy K_0, ensemble enstrophy Ω_0, large-eddy-turnover time τ_{to}, ensemble dissipation rate ε_0, Kolmogorov length scale η_0, and the Kolmogorov time scale τ_0 are given as

$$\begin{aligned} K_0 &= \frac{3A_0}{64}\sqrt{2\pi}\kappa_0^5,\ \Omega_0 = \frac{15A_0}{256}\sqrt{2\pi}\kappa_0^7,\ \tau_{to} = \sqrt{\frac{32}{A_0}}(2\pi)^{1/4}\kappa_0^{-7/2}, \\ \varepsilon_0 &= 2\frac{\mu_0}{\rho_0}\Omega_0,\ \eta_0 = (\nu_0^3/\varepsilon_0)^{1/4},\ \tau_0 = (\nu_0/\varepsilon_0)^{1/2}. \end{aligned} \tag{2}$$

For decaying compressible isotropic turbulence, the root-mean-square pressure fluctuations p_{rms}, and turbulent kinetic energy K are defined as

$$\begin{aligned} p_{rms} &= \sqrt{\langle (p - \langle p\rangle)^2\rangle}, \\ K &= \frac{1}{2}\langle \rho \boldsymbol{U}\cdot\boldsymbol{U}\rangle . \end{aligned} \tag{3}$$

The evolution of turbulent kinetic energy is of interest since it is a fundamental benchmark in the incompressible and compressible turbulence modeling [3,12,47]. In this study, the ensemble budget of turbulent kinetic energy is computed and analyzed, as the decay of the ensemble turbulent kinetic energy can be described approximately by [15]

$$\begin{aligned} \frac{\mathrm{d}\langle K\rangle}{\mathrm{d}t} &= -\varepsilon + \langle p\theta\rangle , \\ \varepsilon &= \varepsilon_s + \varepsilon_d, \\ \chi &= \varepsilon_d/\varepsilon_s, \end{aligned} \tag{4}$$

where $\varepsilon_s = \langle \mu\omega_i\omega_i\rangle$ is the ensemble solenoidal dissipation rate, $\varepsilon_d = \left\langle 4\mu\theta^2/3\right\rangle$ is the ensemble dilational dissipation rate, χ is the ratio of ensemble solenoidal dissipation rate over the ensemble dilational dissipation rate, $\langle p\theta\rangle$ is the ensemble pressure-dilation transfer, $\omega_i = \epsilon_{ijk}\partial U_k/\partial x_j$ is the fluctuating vorticity, ϵ_{ijk} is the alternating tensor, and $\theta = \nabla\cdot\boldsymbol{U}$ is the fluctuating divergence of velocity.

In this section, the DNS study of decaying supersonic isotropic turbulence at a fixed initial turbulent Mach number $Ma_t = 2.0$ with Taylor microscale Reynolds number $Re_\lambda = 72$ and 120 are implemented. Incorporating the two-stage fourth-order temporal discretization and fifth-order WENO-Z spatial reconstruction [49], the high-order gas-kinetic scheme is adopted in the computation, and more details of HGKS can be found in Refs. [8,39,40]. Firstly, the grid size and time step which are guided by previous criterion of HGKS [8] are adopted for the simulation of the decaying supersonic isotropic turbulence in Appendix A. Numerical tests with the initial turbulent Mach number $Ma_t = 1.6$ and initial Taylor microscale Reynolds number $Re_\lambda = 72$ are performed with such a criterion. Appendix A shows that the minimum spatial resolution parameter $\kappa_{max}\eta_0 \geq 2.71$ and the maximum temporal resolution parameter $\Delta t_{ini}/\tau_{to} \leq 5.58/1000$ are adequate to resolve the decaying supersonic isotropic turbulence. For the supersonic isotropic turbulence, guided by such criterion [8], the details of numerical tests R_1 and R_2 are given in Table 1. Due to the strong discontinuities in flow field, the case with $Ma_t = 2.0$ is very challenging, which brings difficulties for the numerical simulation. Numerical results are rarely reported by the classical methods under finite volume and finite difference framework. More studies on the high-order scheme still need be conducted in the future.

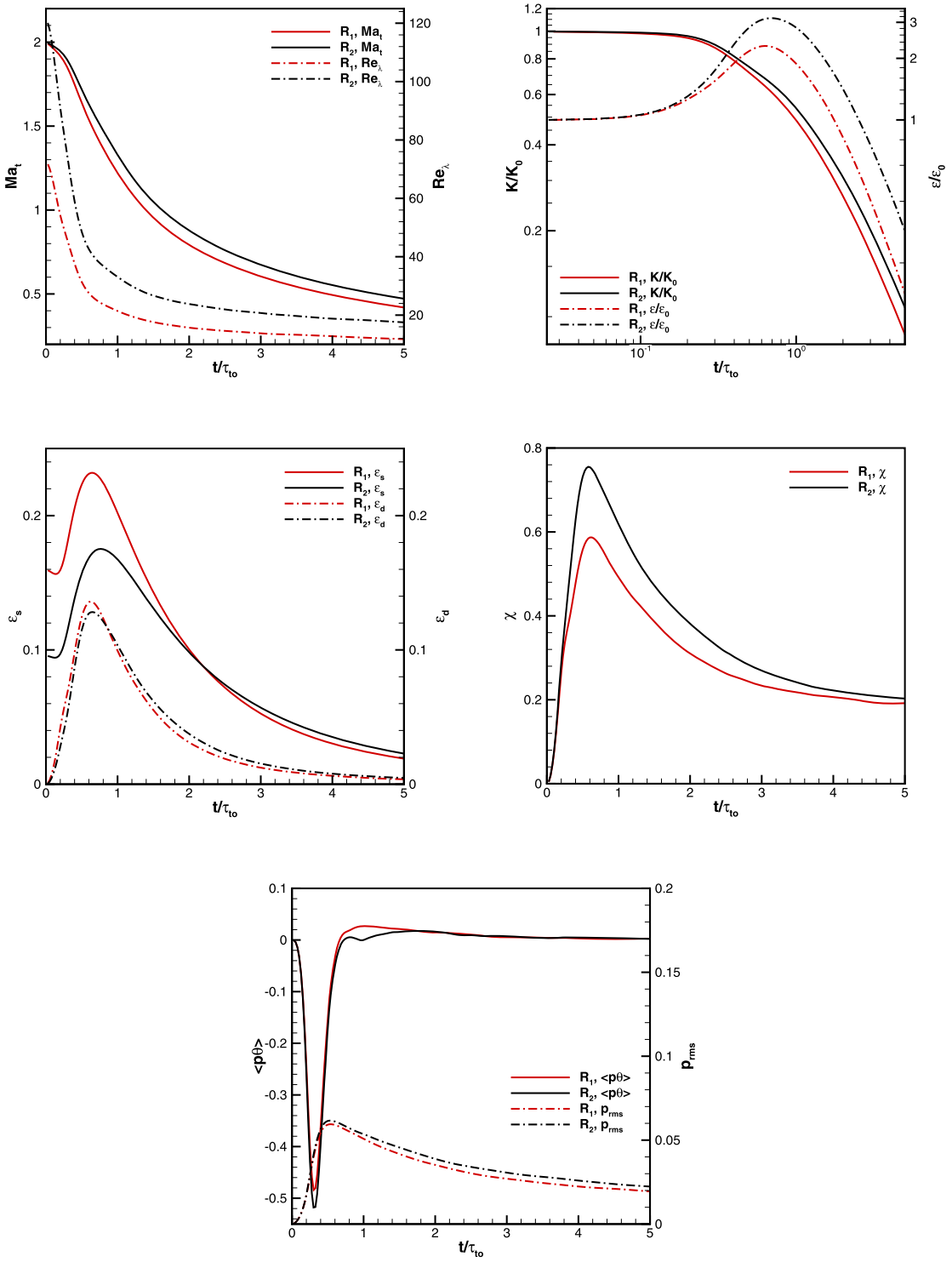

Fig. 1. Time history of Ma_t, Re_λ, K/K_0, $\varepsilon/\varepsilon_0$, ε_s, ε_d, χ, $\langle p\theta \rangle$ and p_{rms} for R_1 and R_2.

The time history of statistical quantities in Eq. (3) and Eq. (4) are presented in Fig. 1. The ensemble turbulent Mach number Ma_t and Taylor microscale Reynolds number Re_λ decay monotonically. During the early stage, Re_λ decays very fast. Up to $t/\tau_{to} = 1.0$, the Taylor microscale Reynolds number Re_λ is approximate 20% of the initial values. Meanwhile, the ensemble dissipation rate ε reaches its maximum, which is around 3 times of ε_0. Obviously, the peak ensemble dilational dissipation rate ε_d is approximately half of the peak ensemble solenoidal dissipation rate ε_s. More specifically, the ratio

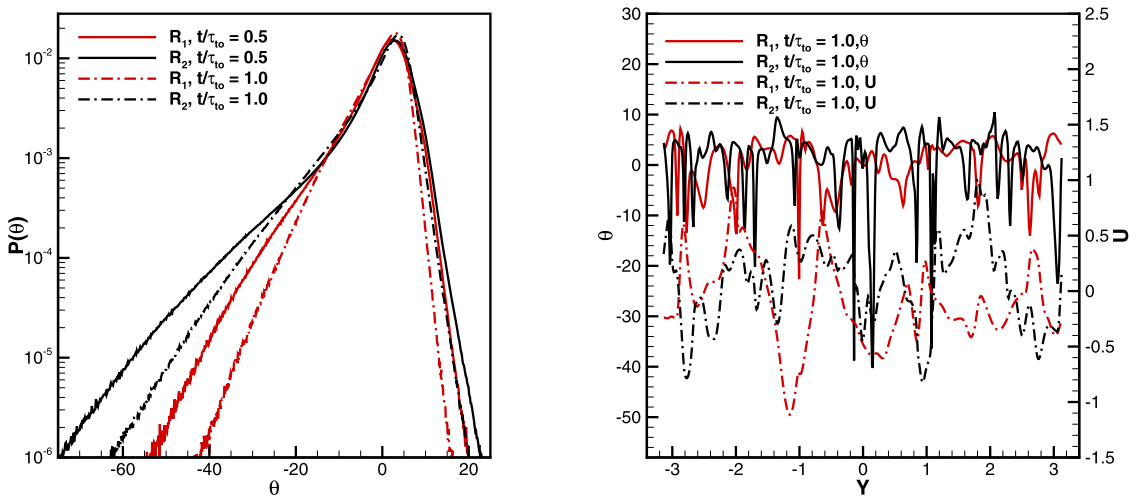

Fig. 2. PDF of dilation θ, x-direction velocity component U and dilation θ along $x = 0$ and $z = 0$ at $t/\tau_{to} = 0.5$ and $t/\tau_{to} = 1.0$ for R_1 and R_2.

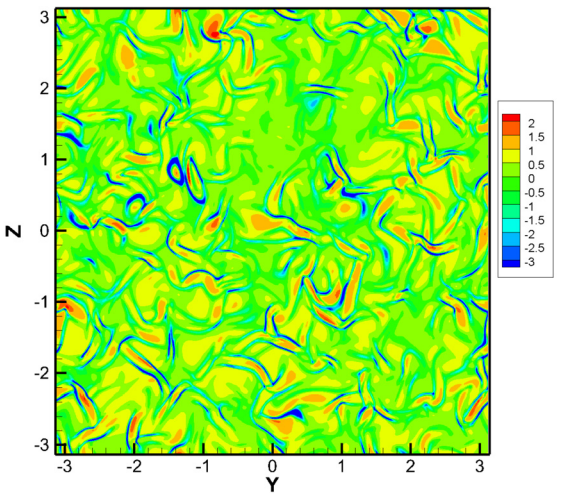

Fig. 3. Contour of normalized dilation $\theta/\langle\theta\rangle^*$ at $x = 0$ at $t/\tau_{to} = 0.5$ for R_1. (For interpretation of the colors in the figure(s), the reader is referred to the web version of this article.)

of ensemble solenoidal dissipation rate over the ensemble dilational dissipation rate $\chi = \varepsilon_d/\varepsilon_s$ is larger than 0.3 during $0.3 \le t/\tau_{to} \le 2$. A large value of χ has significant influence on the current decaying supersonic isotropic turbulence from the contribution of the compressibility. In addition, the ensemble dilational dissipation rate depends on Re_λ slightly, which confirms the previous analysis [8]. Root-mean-square pressure fluctuations p_{rms} reaches its maximum value around $t/\tau_{to} = 0.6$, corresponding to the peak ensemble dilational dissipation rate. During the early stage of the decaying supersonic isotropic turbulence, the ensemble pressure-dilation term can be on the same order of ensemble total dissipation rate [45]. The transfer of turbulent kinetic energy into internal energy cannot be neglected as the case of forced supersonic isotropic turbulence [32]. After $t/\tau_{to} \approx 1.0$, $\langle p\theta\rangle$ changes signs during the evolution and preserves small but positive value.

The probability density functions (PDF) of dilation θ, x-direction velocity component U and dilation θ along $x = 0$ and $z = 0$ at $t/\tau_{to} = 0.5$ and $t/\tau_{to} = 1.0$ for R_1 and R_2 are presented in Fig. 2. All PDFs of dilation θ in Fig. 2 are obtained by dividing the dilation range into 1000 equivalent intervals. All PDFs of dilation show strong negative tails, which are the most significant flow structure of compressible isotropic turbulence resulting from the shocklets [8–10]. The x-direction velocity component U and dilation θ along the $x = 0$ and $z = 0$ indicate that the strong shocklets and high expansion regions appear frequently and randomly. Contour of normalized dilation $\theta/\langle\theta\rangle^*$ at $t/\tau_{to} = 0.5$ of R_1 is presented in Fig. 3. Contour of normalized dilation shows very different behavior between the compression and expansion motion, where $\langle\theta\rangle^*$ is the root-mean-square dilation. Strong compression regions with $\theta/\langle\theta\rangle^* \le -3$ are usually recognized as shocklets [45]. These random distributed shocklets and high expansion region lead to strong spatial gradient in flow fields, which pose much greater challenge for high-order schemes when implementing DNS for isotropic turbulence in supersonic regime. DNS on a much higher initial turbulent Mach number up to $Ma_t = 2.0$ confirms the super robustness of the HGKS. Based on the

high-fidelity DNS data, the coarse-grained analysis for compressible SGS turbulent kinetic energy will be implemented for constructing the compressible one-equation SGS model.

3. Coarse-graining analysis of compressible K_{sgs} budget

In this section, the exact compressible SGS turbulent kinetic energy K_{sgs} transport equation will be derived with density weighted filtering process. The Box filter [50,51] is used for the coarse-graining processes of compressible K_{sgs} transport equation on three sets of unresolved grids. Finally, the dominant terms in compressible K_{sgs} transport equation are determined for constructing the compressible one-equation SGS model for high turbulent Mach number flow.

3.1. Compressible K_{sgs} transport equation

For LES models [27,47], after filtering process on unresolved grids, the flow variables can be decomposed into resolved (filtered) and SGS (residual) terms as follows

$$\phi(\boldsymbol{x}) = \overline{\phi}(\boldsymbol{x}) + \phi'(\boldsymbol{x}). \tag{5}$$

The filtered terms are defined as

$$\overline{\phi}(\boldsymbol{x}) = \int_{\Omega} G(\boldsymbol{x}, \boldsymbol{x}', \boldsymbol{l})\phi(\boldsymbol{x}')\mathrm{d}\boldsymbol{x}',$$

where Ω is the filtered domain and $\boldsymbol{l}$ denotes the filter width associated with the wavelength of the smallest scale retained by the coarse-graining operation. The filter function G is defined as

$$G(\boldsymbol{x}, \boldsymbol{x}', \boldsymbol{l}) = \prod_i G_i(x_i, x_i', l_i).$$

The following Box filter [47,50] in physical space is used in this paper

$$G_i(x_i, x_i', l_i) = \begin{cases} 1/l_i, & \text{for } |x_i - x_i'| \le l_i/2, \\ 0, & \text{otherwise}, \end{cases}$$

where l_i is the filter width in the i-direction, and the positive definite kernel of Box filter allows positive SGS turbulent kinetic energy [51]. Various filter-widths $l_i = n\Delta_i$ are used in the following analysis, where Δ_i is the i-direction grid size. In current study, the filter width and the grid size are the same in x, y and z directions. With the filtering process, the one transport equation K_{sgs} of subgrid-scale kinetic energy for incompressible LES [11,12] has been derived.

In the compressible turbulence modeling, to avoid additional subgrid term in the filtered continuity equation, the density-weighted (Favre) filtering [52] is applied, which reads

$$\tilde{\phi} = \frac{\overline{\rho\phi}}{\overline{\rho}}. \tag{6}$$

In this way, the SGS stress τ_{ij} and SGS kinetic energy $\overline{\rho}K_{sgs}$ are defined as

$$\begin{aligned} \tau_{ij} &= \overline{\rho}(\widetilde{U_i U_j} - \widetilde{U}_i\widetilde{U}_j), \\ \overline{\rho}K_{sgs} &= \frac{1}{2}\tau_{kk} = \frac{1}{2}\overline{\rho}(\widetilde{U_k U_k} - \widetilde{U}_k\widetilde{U}_k). \end{aligned} \tag{7}$$

The compressible SGS kinetic energy equation is derived in Appendix B, and the governing equation is given by

$$(\overline{\rho}K_{sgs})_{,t} + (\overline{\rho}K_{sgs}\widetilde{U}_j)_{,j} = P_{sgs} - D_{sgs} + \Pi_{sgs} + T_{sgs}, \tag{8}$$

where P_{sgs} is the production term, D_{sgs} is the dissipation term, Π_{sgs} is the pressure dilation term, and the last term T_{sgs} is the sum of SGS diffusion terms. More specifically, the right-hand-side terms in Eq. (8) can be written as

$$\begin{aligned} P_{sgs} &= -\tau_{ij}\widetilde{S}_{ij}, \\ D_{sgs} &= \overline{\sigma_{ij}U_{i,j}} - \overline{\sigma}_{ij}\widetilde{U}_{i,j}, \\ \Pi_{sgs} &= \overline{pU_{k,k}} - \overline{p}\widetilde{U}_{k,k}, \\ T_{sgs} &= [-\frac{1}{2}\overline{\rho}(\widetilde{U_i U_i U_j} - \widetilde{U_i U_i}\widetilde{U}_j) + \tau_{ij}\widetilde{U}_i + (\overline{\sigma_{ij}U_i} - \overline{\sigma}_{ij}\widetilde{U}_i) - \overline{\rho}R(\widetilde{TU}_j - \tilde{T}\widetilde{U}_j)]_{,j}, \end{aligned} \tag{9}$$

Table 2
Expressions for the right-hand-side terms in compressible K_{sgs} equation.

Symbol	Expression	Symbol	Expression
P	$-\tau_{ij}\widetilde{S}_{ij}$	T_1	$[-\frac{1}{2}\overline{\rho}(\widetilde{U_i U_i U_j} - \widetilde{U_i U_i}\tilde{U}_j)]_{,j}$
D_1	$\overline{\mu}(\widetilde{\omega_i\omega_i} - \tilde{\omega}_i\tilde{\omega}_i)$	T_2	$(\tau_{ij}\tilde{U}_i)_{,j}$
D_2	$4\overline{\mu}(\widetilde{U^2_{k,k}} - \widetilde{U}^2_{k,k})/3$	T_3	$[(\overline{\sigma_{ij}U_i} - \overline{\sigma}_{ij}\tilde{U}_i)]_{,j}$
Π	$\overline{pU_{k,k}} - \overline{p}\widetilde{U}_{k,k}$	T_4	$[-\overline{\rho}R(\widetilde{TU}_j - \tilde{T}\tilde{U}_j)]_{,j}$

Table 3
DNS and filtering LES grids for R_1 and R_2.

	Grid size	$\kappa_{max}\eta_0$		Grid size	$\kappa_{max}\eta_0$
DNS	384^3	2.71	DNS	512^3	2.80
case A_1	192^3	1.36	case B_1	256^3	1.40
case A_2	96^3	0.68	case B_2	128^3	0.70
case A_3	64^3	0.45	case B_3	64^3	0.35

where $\widetilde{S}_{ij} = 1/2(\widetilde{U}_{i,j} + \widetilde{U}_{j,i})$. More details about the derivation of Eq. (8) can be found in Appendix B. The SGS production term $-\tau_{ij}\widetilde{S}_{ij}$ represents the inter-scale transfer associated with the interaction of resolved and unresolved scales. There exists local SGS turbulent kinetic energy backscatter, which illustrates the SGS turbulent kinetic energy transfer from sub-grid scales to resolved scales [32,50]. As presented in Appendix B, the total SGS dissipation rate D_{sgs} can be decomposed into two parts, the SGS solenoidal dissipation rate ε_s^{sgs} and SGS dilational dissipation rate ε_d^{sgs}, as

$$\begin{aligned} \varepsilon_s^{sgs} &= \overline{\mu}(\widetilde{\omega_i\omega_i} - \tilde{\omega}_i\tilde{\omega}_i), \\ \varepsilon_d^{sgs} &= 4\overline{\mu}(\widetilde{U^2_{k,k}} - \widetilde{U}^2_{k,k})/3, \end{aligned} \tag{10}$$

where $\omega_i = \epsilon_{ijk}U_{k,j}$ is the resolved vorticity and $\tilde{\omega}_i = \epsilon_{ijk}\widetilde{U}_{k,j}$ is the filtered one with the permutation symbol ϵ_{ijk}. There is a slight difference between Eq. (10) and Eq.(3.8) in the reference [25]. Restricting the analysis to the linear Kovasznay splitting [53], the solenoidal dissipation is associated entirely with the vorticity mode, whereas the dilational dissipation is mainly due to the acoustic mode in the absence of significant entropy source [5]. The SGS pressure-dilation term Π_{sgs} is related to the redistribution of K_{sgs} in the flow fields of compressible turbulence. The pressure-dilation term reduces to 0 in the incompressible limit. T_{sgs} is the sum of all SGS diffusion terms, which are usually grouped and modeled together for both incompressible and compressible turbulence models [6,21]. In this paper, in order to determine the dominant SGS diffusion term, all SGS diffusion terms are analyzed in detail. According to Eq. (9), the right-hand-side terms of Eq. (8) are classified in Table 2. With the Favre filtering process on unresolved grids, the analysis of dominant source terms and SGS diffusion terms will be presented in the following section.

3.2. Coarse-graining analysis of compressible K_{sgs} transport equation

The DNS and filtering LES grids for R_1 and R_2 are presented in Table 3. The discretization method of spatial derivatives plays a key role in analyzing the budget of compressible K_{sgs} transport equation. In current paper, to be consistent with the HGKS calculation [8], the fifth-order WENO-Z reconstruction [49] is adopted in computing the spatial derivatives of flow variables, and details are given in Appendix C.

The coarse-grained compressible K_{sgs} budgets P, D_1, D_2 and Π in Eq. (9) for A_1, A_2, A_3 and B_1, B_2, B_3 are presented in Fig. 4. The budgets are computed in the domain average, and the spatial derivatives are obtained by the WENO-Z reconstruction as the Appendix C. The domain average is defined as $||x|| = \sum_{i=1}^{N} x_i/N$. As shown in Fig. 4, all unresolved source terms are dominant terms within $0 \le t/\tau_{to} \le 3.0$. Obviously, the SGS production term $-\tau_{ij}\widetilde{S}_{ij}$ is the most important one, considering the largest positive magnitude among the four source terms. The SGS production term P is positive, which represents the forward scattering of ensemble SGS kinetic energy. The ensemble SGS dilational dissipation rate D_2 is more than half of the ensemble SGS solenoidal dissipation rate D_1. Compared with the incompressible turbulence system, the dilational dissipation rate cannot be neglected in supersonic turbulence. The coarse-graining analysis on the SGS dissipation rate for supersonic isotropic turbulence agrees with previous conclusion on compressible turbulence at a moderate turbulent Mach number ($Ma_t = 0.52$) [31]. In addition, with the coarser grids, the ratio of D_2 and D_1 becomes larger. When modeling the SGS dissipation rate, the one-equation SGS model for compressible LES should consider the grids effect [23–25]. The negative values of Π represent the ensemble SGS pressure-dilation term as the sink for SGS kinetic energy. Different from Fig. 1, the SGS pressure-dilation term Π doesn't change signs during the evolution and always preserves negative value on unresolved grids. Especially, the magnitude of SGS pressure-dilation term Π is on the order of unresolved SGS dissipation term within the acoustic time scale τ_a, where acoustic time is defined as $\tau_a = Ma_t\tau_{to}$ [4]. Thus, for decaying supersonic isotropic turbulence, it can be concluded that the SGS pressure-dilation term cannot be neglected as realized previously

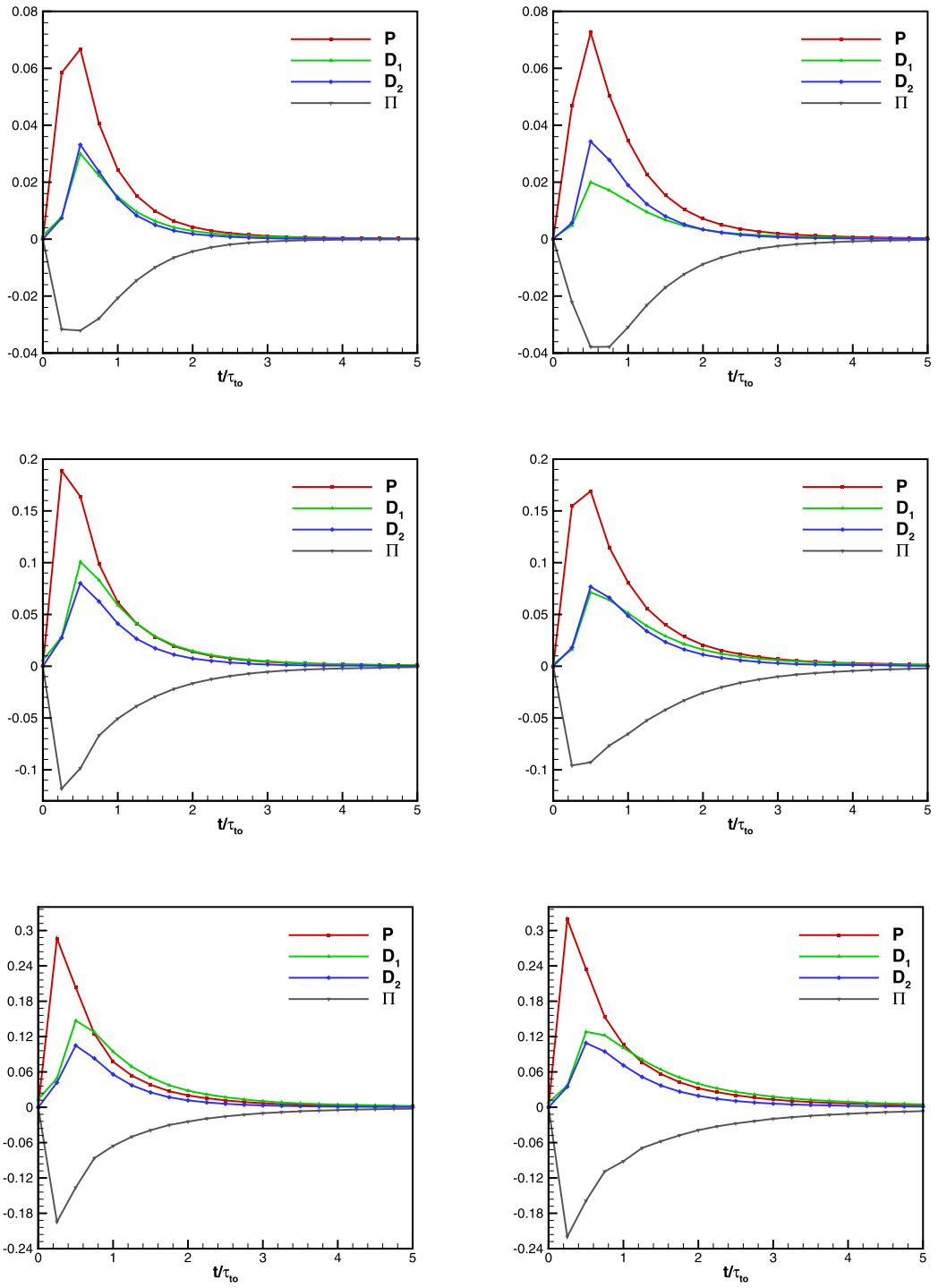

Fig. 4. Coarse-grained compressible K_{sgs} budgets of P, D_1, D_2, and Π for A_1, A_2, A_3 (left column, from the upper row to the bottom row) and B_1, B_2, B_3 (right column, from the upper row to the bottom row).

[23,32]. The literature for modeling SGS pressure-dilation term in subsonic regime can be found in Refs. [16,17,20], where many unknowns remain for supersonic isotropic turbulence. As shown in Fig. 1, the turbulent Mach number $Ma_t \approx 0.7$ and Taylor microscale Reynolds number $Re_\lambda \leq 20$ with $t/\tau_{to} \geq 3.0$, and the resolved ensemble dissipation rate and pressure-dilation rate decrease to a small magnitude. At the same time, on unresolved grids as shown in Fig. 4, the source terms decay to a very small magnitude, which indicate that even the coarsest grids A_3 and B_3 are fine enough to resolve the

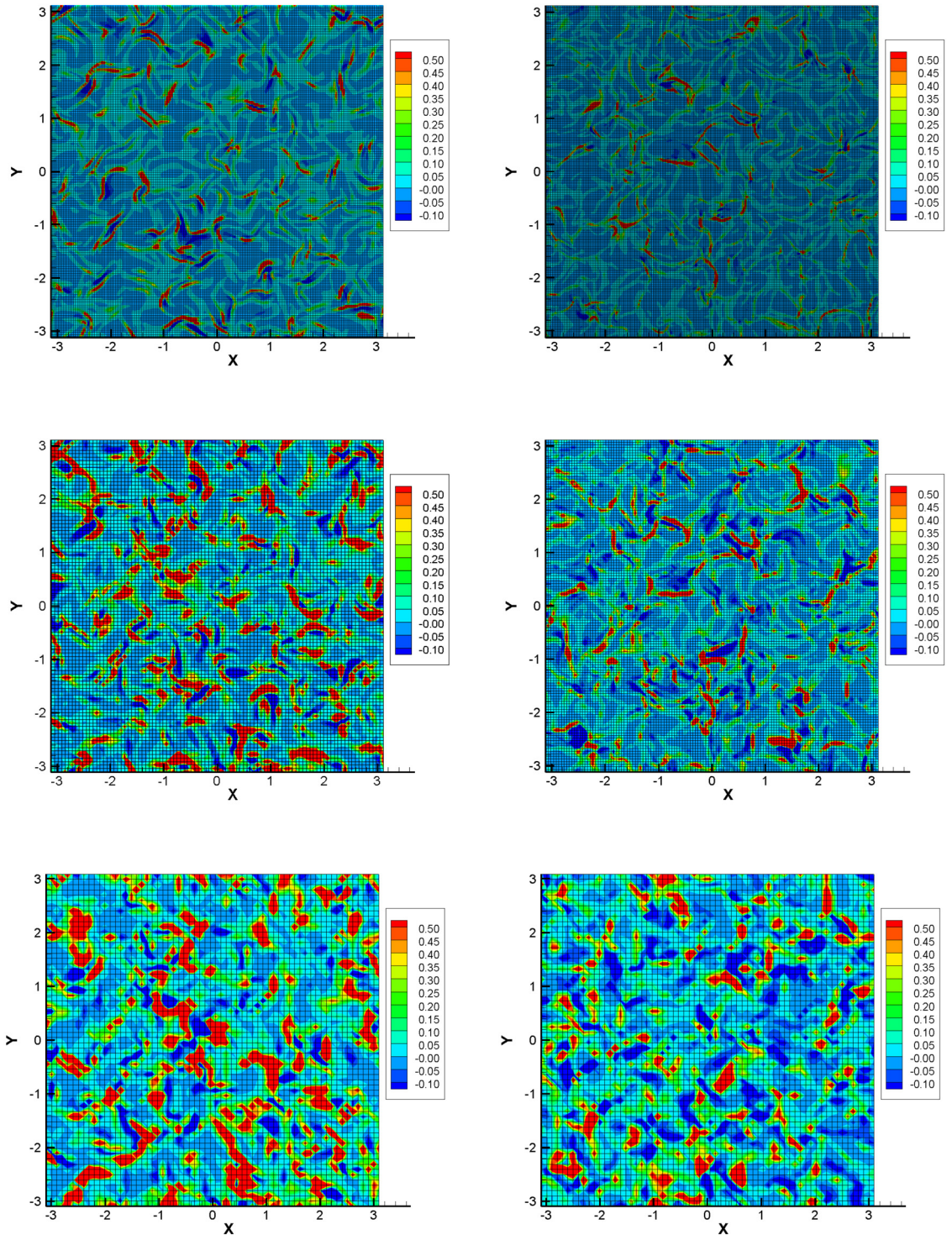

Fig. 5. SGS production term P for A_1, A_2 and A_3 at $t/\tau_{to} = 0.5$ (left), and B_1, B_2 and B_3 at $t/\tau_{to} = 1.0$ (right) at $z = 0$.

flow fields. This behavior is reasonable since the current system is about very small Taylor microscale Reynolds number $Re_\lambda \leq 20$.

The contours of SGS production term P for A_1, A_2, A_3 at $t/\tau_{to} = 0.5$ and B_1, B_2, B_3 at $t/\tau_{to} = 1.0$ at $z = 0$ are presented in Fig. 5. The forward scattering and backscattering coexist [50,32] and randomly distribute on the unresolved grids. The magnitude and portion of positive $-\tau_{ij}\widetilde{S}_{ij}$ are larger than the negative ones, confirming that the ensemble forward scattering

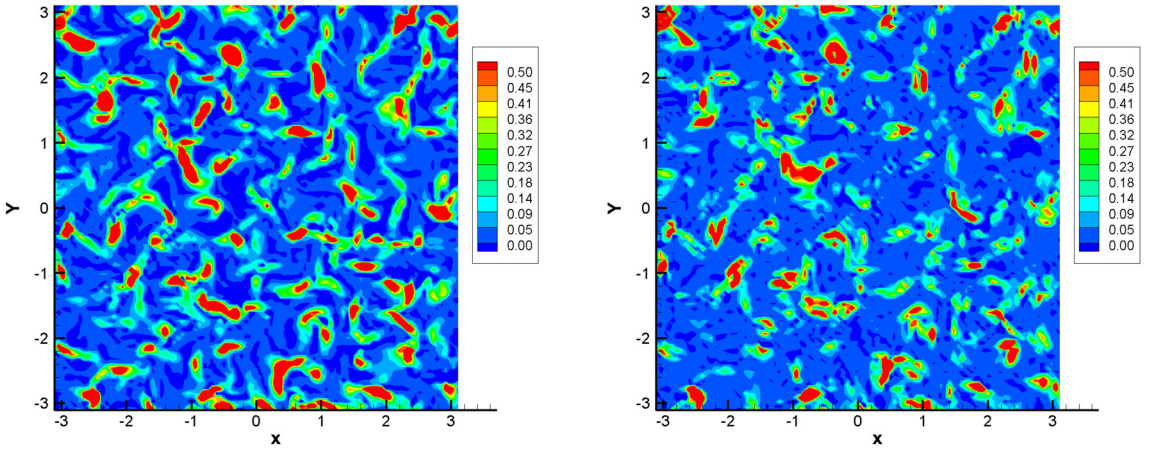

Fig. 6. SGS solenoidal dissipation term D_1 (left), SGS dilational dissipation term D_2 (right) for case A_2 at $t/\tau_{to} = 0.5$ at $z = 0$.

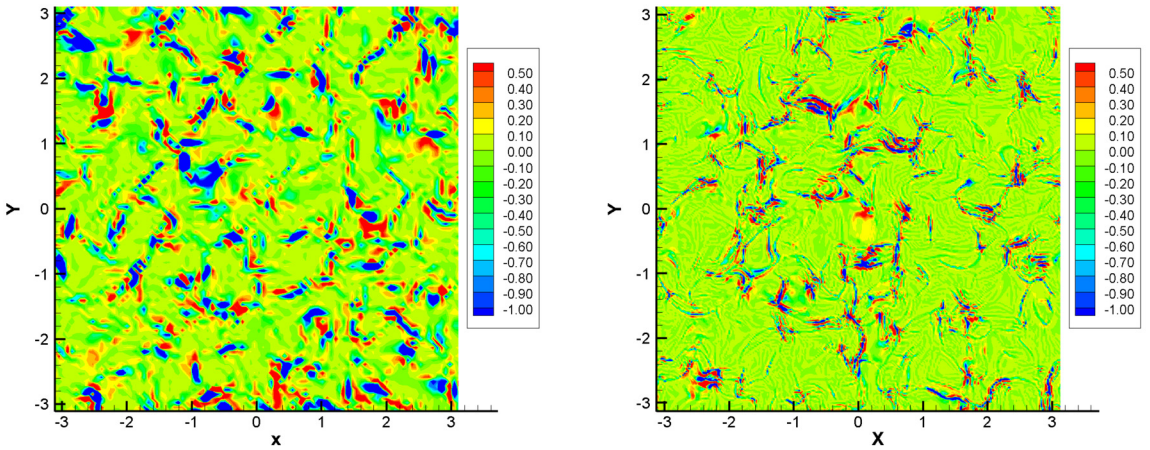

Fig. 7. SGS pressure-dilation transfer term Π for case A_2 at $t/\tau_{to} = 0.5$ (left) and B_1 at $t/\tau_{to} = 1.0$ (right) at $z = 0$.

transfers the SGS turbulent kinetic energy from the resolved scales to the sub-grid scales. To model the backscattering process in supersonic isotropic turbulence, the dynamic approach is recommended [25,54]. Contours of SGS solenoidal dissipation term D_1 and dilational dissipation term D_2 for A_2 at $t/\tau_{to} = 0.5$ and B_1 at $t/\tau_{to} = 1.0$ at $z = 0$ are presented in Fig. 6. The dissipation rate is non-negative, and the high similarity between the D_1 and D_2 in spatial distribution is confirmed [25]. Previous modeling [15] on dilational dissipation rate $D_2 \propto Ma_t^2 D_1$ may still work in this supersonic isotropic turbulence, which will be studied in the following paper. Fig. 7 shows the SGS pressure-dilation transfer term Π for case A_2 at $t/\tau_{to} = 0.5$ and B_1 at $t/\tau_{to} = 1.0$ at $z = 0$. It is observed that the magnitude and portion of negative Π are larger than the positive ones, which confirm the absorption of K_{sgs} from the ensemble SGS pressure-dilation term, as shown in Fig. 4.

In previous study, the SGS diffusion terms are grouped and modeled together by the gradient-type models for both incompressible and compressible turbulent flows [6,21]. To study the delicate behavior of the SGS diffusion terms in the SGS kinetic energy equation, the coarse-graining analysis of dominant SGS diffusion terms is implemented. The coarse-grained budget of SGS diffusion terms T_1, T_2, T_3 and T_4 for A_1, A_2, A_3 and B_1, B_2, B_3 are presented in Fig. 8. The spatial derivatives are obtained by the WENO-Z reconstruction as that in the Appendix C. Because the ensemble of the sum of transport terms is equivalent to 0, the L_2 norm is applied in analyzing the SGS diffusion terms, where L_2 norm is defined by $||x||_{L_2} = (\sum_{i=1}^{N} x_i^2)^{0.5}/N$. As shown in Fig. 8, within $0 \le t/\tau_{to} \le 2.0$, both the fluctuation velocity triple correlation term T_1 and the pressure-velocity correlation term T_4 become dominant terms. T_1 and T_4 are about 10 times larger than the negligible terms T_2 and T_3, i.e., $\|T_1\|_{L_2} \approx 10\|T_3\|_{L_2}$. The coarse-graining analysis on SGS diffusion terms for supersonic isotropic turbulence agrees with previous conclusion on subsonic isotropic turbulence [29], i.e. the priori tests of mixing layer up to Mach numbers 0.6. When $t/\tau_{to} \ge 3.0$, all SGS diffusion terms T_1-T_4 decay to a very mall magnitude as that in Fig. 4. This is because of the very small Taylor microscale Reynolds number $Re_\lambda \le 20$, even the coarsest grids A_3 and B_3 are fine enough to resolve the flowfields.

The contours of SGS diffusion terms T_1, T_2, T_3 and T_4 for case A_2 at $t/\tau_{to} = 0.5$ are presented in Fig. 9, in which the fluctuation velocity triple correlation term T_1 and the pressure-velocity correlation term T_4 behave more importantly than

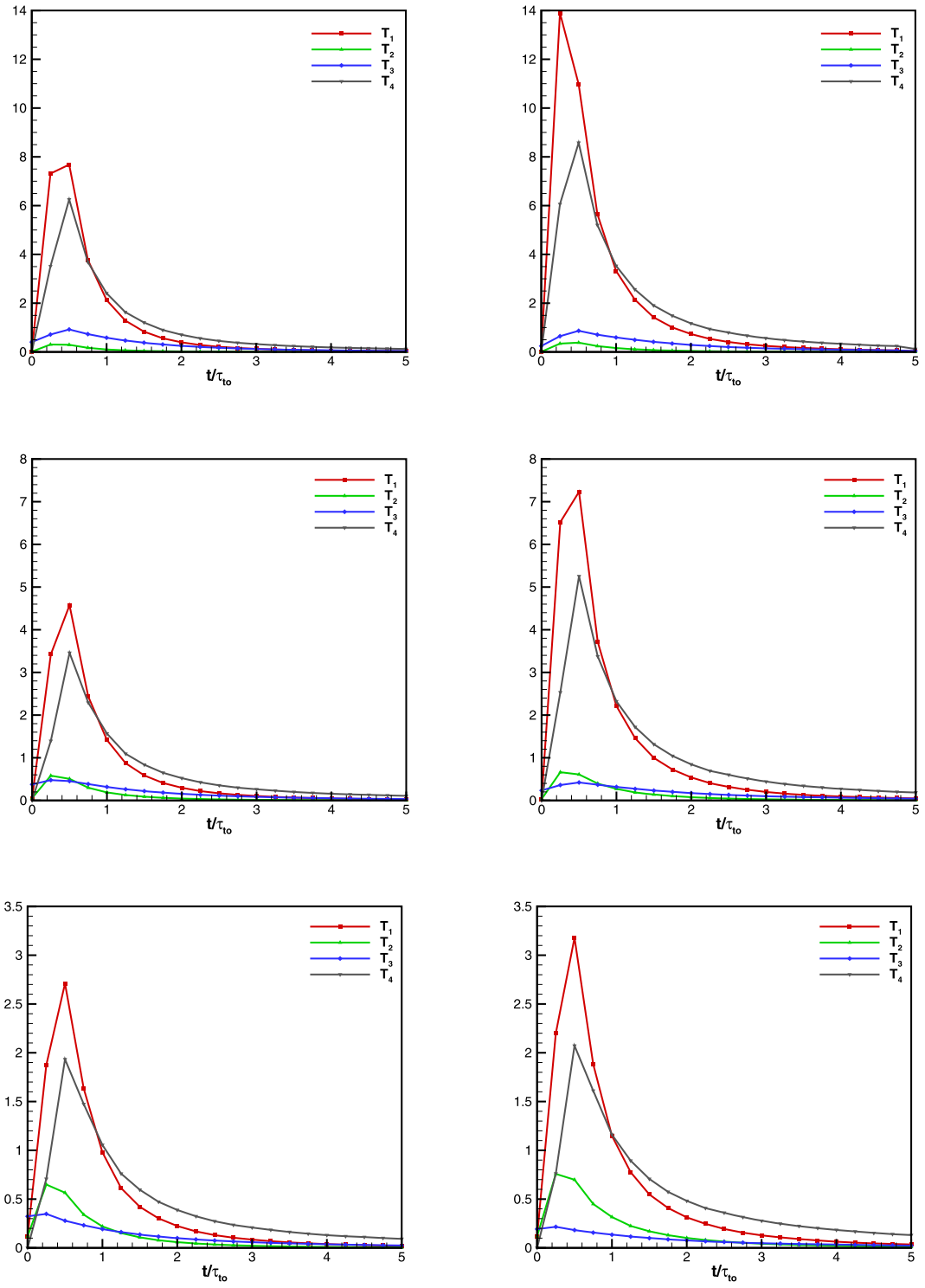

Fig. 8. Coarse-grained budgets of SGS diffusion terms T_1, T_2, T_3 and T_4 for cases A_1, A_2, A_3 (left column, from the upper row to the bottom row) and B_1, B_2, B_3 (right column, from the upper row to the bottom row).

the SGS diffusion terms T_2 and T_3. To be of interest, the fluctuation velocity triple correlation term T_1 and the pressure-velocity correlation term T_4 are found to be highly correlated. To further study the correlation, Kullback-Leibler divergence (KLD) [55] is introduced to measure the relationship of statistical behavior, namely, the correlation between two PDFs of

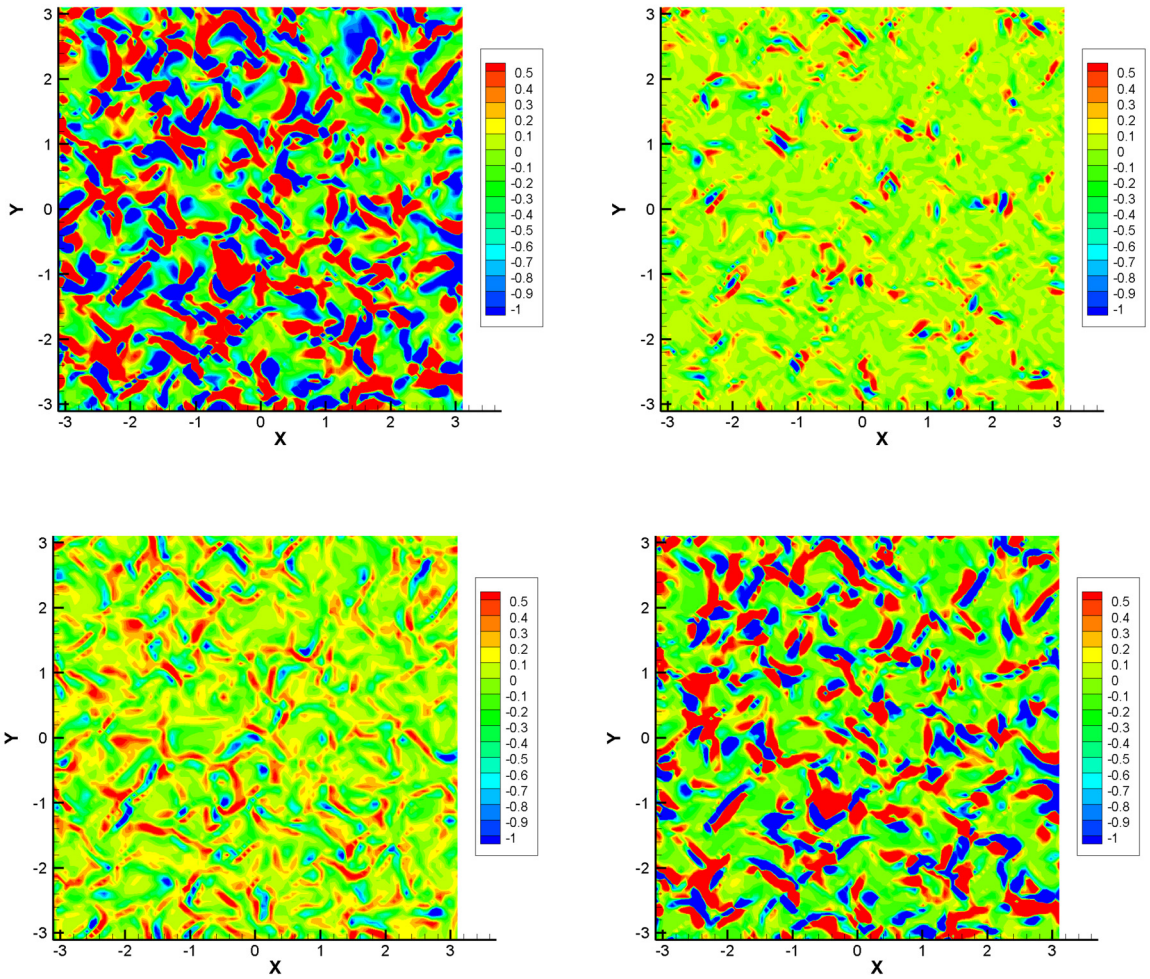

Fig. 9. SGS diffusion terms T_1, T_2 (upper row), T_3 and T_4 (lower row) diffusion terms for case A_2 at $t/\tau_{to} = 0.5$ at $z = 0$.

SGS diffusion terms. In addition, the linear correlation coefficient is used to measure the spatial correlation of four SGS diffusion terms. The KLD and linear correlation coefficient are defined as

$$\begin{aligned} D_{kl}(\boldsymbol{T}_i||\boldsymbol{T}_1) &= \sum_j \boldsymbol{T}_i(j) \log \frac{\boldsymbol{T}_i(j)}{\boldsymbol{T}_1(j)}, \\ Coe(\boldsymbol{T}_i||\boldsymbol{T}_1) &= \frac{\mathrm{cov}(\boldsymbol{T}_i, \boldsymbol{T}_1)}{\sigma_{\boldsymbol{T}_i}\sigma_{\boldsymbol{T}_1}}, \end{aligned} \tag{11}$$

where $\boldsymbol{T}_i$ is the PDF of SGS diffusion term T_i, $\mathrm{cov}(\cdot,\cdot)$ represents the covariance of two random variables, and $\sigma_{\cdot}$ is standard deviation of one random variables. All PDFs of T_i in this paper are obtained by dividing the range of the SGS diffusion term into 1000 equivalent intervals. History of KLD and linear correlation coefficient among the SGS diffusion terms T_1, T_2, T_3 and T_4 for case B_1, B_2, B_3 are presented in Fig. 10. The coarser grid is, the smaller magnitude of KLD is, indicating the much closer relation between T_i and T_1 on coarser grid. As different grids show different order of magnitude of KLD, it indicates that the grid effect should be considered in constructing the one-equation SGS model. The linear correlation coefficient confirms the high correlation between T_1 and T_4, which shows the strong coupling between the kinematics and thermodynamics in current supersonic isotropic turbulence. When using the dynamic approach [28] to determine the dynamic coefficients for modeling SGS diffusion term [25], both T_1 and T_4 should participate in the dynamic modeling, instead of only considering T_1 as incompressible one-equation SGS model [13,14].

In summary, the classification of terms in the compressible K_{sgs} equation is presented in Table 4. Compared with incompressible turbulent system [11], the current study points out the additional dominant terms D_2, Π and T_4, which deserve further study for the modeling of high Mach number turbulence. The compressible K_{sgs} transport equation is analyzed, which paves the way for modeling the unknowns in compressible one-equation SGS model. Subsequent paper will focus on the compressible one-equation SGS model for high Mach number turbulent flow.

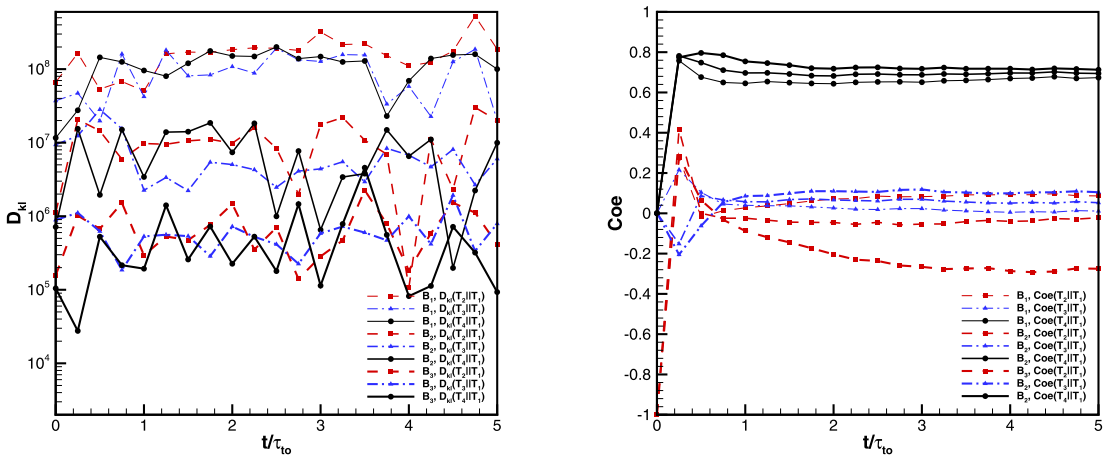

Fig. 10. History of Kullback-Leibler divergence (left) and linear correlation coefficient (right) among the SGS diffusion terms T_1, T_2, T_3 and T_4 for cases B_1-B_3.

Table 4
Classification of terms in incompressible and compressible K_{sgs} equation.

Category	Current compressible system	Incompressible system
Dominant terms	P, D_1, D_2, Π, T_1, T_4	P, D_1, T_1
Negligible terms	T_2, T_3	D_2, Π, T_2, T_3, T_4

4. Conclusion

In this paper, the coarse-graining analysis of compressible SGS turbulent kinetic energy budget K_{sgs} is fully analyzed for constructing one-equation SGS model of compressible LES at high turbulent Mach number. DNS on a much higher initial turbulent Mach number up to $Ma_t = 2.0$ is performed by the HGKS, which provides a high-fidelity DNS data for coarse-graining analysis. The exact compressible SGS turbulent kinetic energy K_{sgs} transport equation is derived by the Favre filtering procedures, and the coarse-graining processes are implemented on the unresolved grids. The coarse-graining analysis of compressible K_{sgs} budgets shows that all unresolved source terms are dominant terms, i.e., SGS production term, solenoidal dissipation term, dilational dissipation term, and pressure-dilation term. Especially, for the decaying supersonic isotropic turbulence, the SGS pressure-dilation term plays a significant role in SGS turbulent kinetic energy transfer, which cannot be neglected. The coarse-graining analysis of SGS diffusion terms shows both the fluctuation velocity correlation term and the pressure-velocity correlation term are also the dominant terms. The pressure-velocity correlation term should participate in the dynamic modeling when determining the dynamic coefficients for modeling SGS diffusion term. The current coarse-graining analysis gives an indication of the order of magnitude of all unresolved terms in compressible K_{sgs} budget, which provides a solid basis for compressible one-equation SGS model. The compressible one-equation SGS model under the non-equilibrium time-relaxation gas-kinetic framework for the turbulence study at high turbulent Mach number will be presented in the subsequent paper.

CRediT authorship contribution statement

Our group has been working on the topic for a long time. The research output is coming from our joint effort. All authors read and approved the final manuscript.

Declaration of competing interest

The authors declare that they have no known competing financial interests or personal relationships that could have appeared to influence the work reported in this paper.

Acknowledgements

The authors thank the reviewers for their critical comments and helpful suggestions. The current research is supported by National Science Foundation of China (11701038, 11772281, 91852114), the Fundamental Research Funds for the Central Universities (2018NTST19), and the National Numerical Windtunnel project. The authors would like to thank TianHe-II in Guangzhou for providing high performance computational resources.

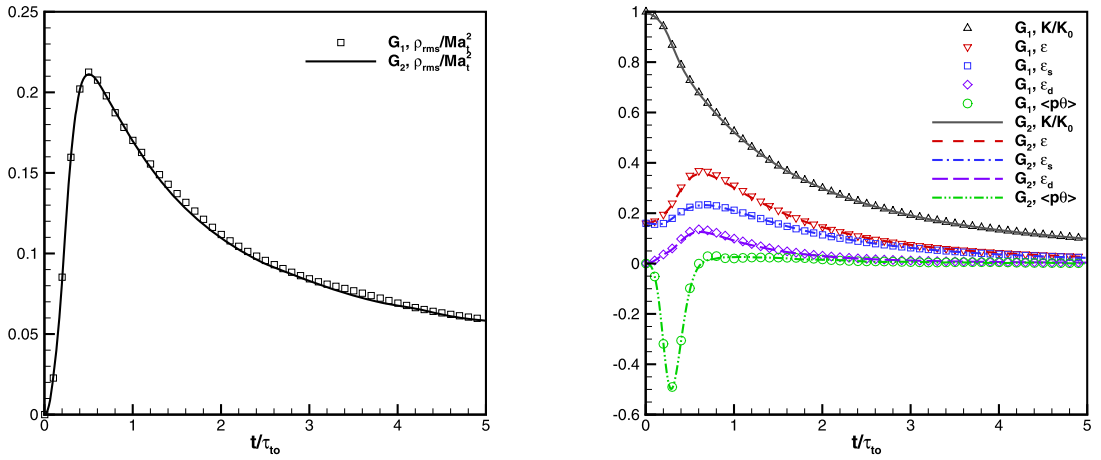

Fig. 11. Grid convergence study: time history of ρ_{rms}/Ma_t^2, K/K_0, ε, ε_s, ε_d and $\langle p\theta \rangle$ for decaying supersonic isotropic turbulent with $Ma_t = 1.6$ and $Re_\lambda = 72$ on uniform grids with 384^3 and 512^3 cells. ($\rho_{rms} = \sqrt{\langle(\rho - \langle\rho\rangle)^2\rangle}$ represents the root-mean-square density fluctuation.)

Appendix A. Grid convergence study for decaying supersonic isotropic turbulence

For supersonic isotropic turbulence, the grid convergence study with the initial turbulent Mach number $Ma_t = 1.6$ and initial Taylor microscale Reynolds number $Re_\lambda = 72$ is implemented. Case G_2 with 384^3 cells has already met previous criterion for DNS [8], namely, the minimum spatial resolution parameter $\kappa_{max}\eta_0 \geq 2.71$ and the maximum temporal resolution parameter $\Delta t_{ini}/\tau_{to} \leq 5.58/1000$. Case G_1 with 512^3 cells and smaller time step than that in G_2 is the current refined mesh test. As shown in Fig. 11, the key statistical quantities on uniform grids with 384^3 cells match well with those on uniform grids with 512^3 cells. It can be concluded that the grid resolution guided by such criterion for DNS in Ref. [8] is adequate for resolving the decaying supersonic isotropic turbulence.

Appendix B. Derivation of compressible K_{sgs} transport equation

For the filtering operator Eq. (5), the following two properties, namely linearity and commutation with differentiation [47] are required as

$$\begin{aligned} \overline{\phi + \varphi} &= \overline{\phi} + \overline{\varphi}, \\ \overline{\frac{\partial \phi}{\partial s}} &= \frac{\partial \overline{\phi}}{\partial s}, \end{aligned} \tag{12}$$

where $s = \boldsymbol{x}, t$. To avoid subgrid term appearing in the filtered continuity equation, the Favre filtering [52] as Eq. (6) is considered. For the Favre filtering, only the linearity has been inherited as

$$\widetilde{\phi + \varphi} = \widetilde{\phi} + \widetilde{\varphi}. \tag{13}$$

It should be noticed that the commutation with differentiation doesn't apply to the Favre filtering. The SGS kinetic energy equation can be derived by subtracting the product of the Favre-filtered velocity and the filtered momentum equation from the filtered product of the velocity and momentum equation [25]

$$\overline{U_i \times [(\rho U_i)_{,t} + (\rho U_i U_j)_{,j} + p_{,i} - (\sigma_{ij})_{,j}]} - \widetilde{U}_i \times \overline{(\rho U_i)_{,t} + (\rho U_i U_j)_{,j} + p_{,i} - (\sigma_{ij})_{,j}} = 0, \tag{14}$$

where ρ is the density, U_i is the velocity component, $p = \rho RT$ is the pressure, and T is the temperature, and R is the gas constant. Ignoring the bulk viscosity, the viscous stress σ_{ij} is given by

$$\sigma_{ij} = \mu\left(U_{i,j} + U_{j,i} - \frac{2}{3}U_{k,k}\delta_{ij}\right),$$

where μ is the molecular viscosity, and δ_{ij} is the Kronecker symbol. Based on properties of filtering in Eq. (12) and Eq. (13), Eq. (14) can be rearranged term by term to derive SGS kinetic energy equation.

The first term L_1 is defined and grouped as

$$L_1 = \overline{U_i \times (\rho U_i)_{,t}} - \widetilde{U}_i \times \overline{(\rho U_i)_{,t}} = [\overline{\rho}(\widetilde{U_i U_i} - \widetilde{U}_i \widetilde{U}_i)]_{,t} - (\overline{\rho U_i U_{i,t}} - \overline{\rho}\widetilde{U}_i \widetilde{U}_{i,t}). \tag{15}$$

The continuity and momentum equation can be used to replace $U_{i,t}$ as $\rho U_{i,t} = (\rho U_i)_{,t} - U_i \rho_{,t}$. Similarly, the filtered continuity equation and filtered momentum equation can be used to replace $\widetilde{U}_{i,t}$. Plugging above replacements into Eq. (15), L_1 can be rewritten as

$$\begin{aligned} L_1 =& [\overline{\rho}(\widetilde{U_i U_i} - \widetilde{U}_i \widetilde{U}_i)]_{,t} + \overline{U_i \times [(\rho U_i U_j)_{,j} + p_{,i} - (\sigma_{ij})_{,j}]} \\ & - \widetilde{U}_i \times \overline{(\rho U_i U_j)_{,j} + p_{,i} - (\sigma_{ij})_{,j}} - [\overline{U_i^2 (\rho U_j)_{,j}} - \widetilde{U}_i^2 (\overline{\rho}\widetilde{U}_j)_{,j}]. \end{aligned}$$

With the definition of SGS kinetic energy $\overline{\rho}(\widetilde{U_k U_k} - \widetilde{U}_k \widetilde{U}_k) = 2\overline{\rho} K_{sgs}$ in Eq. (7), plugging L_1 into Eq. (14), leads to

$$\begin{aligned} 2(\overline{\rho} K_{sgs})_{,t} + 2 \left\{ \overline{U_i \times [(\rho U_i U_j)_{,j} + p_{,i} - (\sigma_{ij})_{,j}]} - \widetilde{U}_i \times \overline{(\rho U_i U_j)_{,j} + p_{,i} - (\sigma_{ij})_{,j}} \right\} \\ = \overline{U_i^2 (\rho U_j)_{,j}} - \widetilde{U}_i^2 (\overline{\rho}\widetilde{U}_j)_{,j}. \end{aligned} \tag{16}$$

The second term L_2 can be defined and rewritten as

$$\begin{aligned} L_2 =& \overline{U_i \times (\rho U_i U_j)_{,j}} - \widetilde{U}_i \times \overline{(\rho U_i U_j)_{,j}} \\ =& \overline{(\rho U_i U_i U_j)_{,j} - \rho U_i U_j U_{i,j}} - \widetilde{U}_i \times [(\overline{\rho}\widetilde{U}_i \widetilde{U}_j)_{,j} + (\tau_{ij})_{,j}], \end{aligned} \tag{17}$$

where $\tau_{ij} = \overline{\rho}(\widetilde{U_i U_j} - \tilde{u}_i \tilde{u}_j)$ as defined in Eq. (7). Combining L_2 and the right-hand-side term in Eq. (16), we have

$$\begin{aligned} L_3 =& 2 \times L_2 - [\overline{U_i^2 (\rho U_j)_{,j}} - \widetilde{U}_i^2 (\overline{\rho}\widetilde{U}_j)_{,j}] \\ =& 2(\overline{\rho} K_{sgs} \widetilde{U}_j)_{,j} + [\overline{\rho}(\widetilde{U_i U_i U_j} - \widetilde{U_i U_i}\widetilde{U}_j)]_{,j} - 2\widetilde{U}_i (\tau_{ij})_{,j}. \end{aligned}$$

The last term in L_3 can be rewritten as

$$\widetilde{U}_i (\tau_{ij})_{,j} = (\tau_{ij}\widetilde{U}_i)_{,j} - \tau_{ij}\widetilde{U}_{i,j} = (\tau_{ij}\widetilde{U}_i)_{,j} - \tau_{ij}\widetilde{S}_{ij},$$

where the decomposition $\widetilde{U}_{i,j} = \widetilde{S}_{ij} + \widetilde{\Omega}_{ij}$ is involved, $\widetilde{S}_{ij} = (\widetilde{U}_{i,j} + \widetilde{U}_{j,i})/2$ and $\widetilde{\Omega}_{ij} = (\widetilde{U}_{i,j} - \widetilde{U}_{j,i})/2$. $\tau_{ij}\widetilde{\Omega}_{ij} = 0$ because it involves multiplication of a symmetric tensor τ_{ij} by an anti-symmetric tensor $\widetilde{\Omega}_{ij}$. Plugging L_3 into Eq. (16), it leads to

$$\begin{aligned} 2(\overline{\rho} K_{sgs})_{,t} + 2(\overline{\rho} K_{sgs}\widetilde{U}_j)_{,j} + 2 \left\{ \overline{U_i \times [p_{,i} - (\sigma_{ij})_{,j}]} - \widetilde{U}_i \times \overline{p_{,i} - (\sigma_{ij})_{,j}} \right\} \\ = -2\tau_{ij}\widetilde{S}_{ij} - [\overline{\rho}(\widetilde{U_i U_i U_j} - \widetilde{U_i U_i}\widetilde{U}_j)]_{,j} + 2(\tau_{ij}\widetilde{U}_i)_{,j}. \end{aligned} \tag{18}$$

In Eq. (18), substituting $\overline{p} = \overline{\rho} R \tilde{T}$ into pressure-gradient velocity correlation, leads to the following form

$$L_4 = \overline{U_i \times p_{,i}} - \widetilde{U}_i \times \overline{p}_{,i} = [\overline{\rho} R(\widetilde{T U_i} - \widetilde{T}\widetilde{U}_i)]_{,i} - (\overline{p U_{i,i}} - \overline{p}\widetilde{U}_{i,i}).$$

The term L_5 can be designed and decomposed as follows

$$\begin{aligned} L_5 =& \overline{U_i \times (\sigma_{ij})_{,j}} - \widetilde{U}_i \times \overline{(\sigma_{ij})_{,i}} \\ =& (\overline{\sigma_{ij} U_i} - \overline{\sigma}_{ij}\widetilde{U}_i)_{,j} - (\overline{\sigma_{ij} U_{i,j}} - \overline{\sigma}_{ij}\widetilde{U}_{i,j}). \end{aligned}$$

Plugging L_4 and L_5 into Eq. (18), the SGS kinetic energy equation reads

$$\begin{aligned} (\overline{\rho} K_{sgs})_{,t} + (\overline{\rho} K_{sgs}\widetilde{U}_j)_{,j} =& -\tau_{ij}\widetilde{S}_{ij} - (\overline{\sigma_{ij} U_{i,j}} - \overline{\sigma}_{ij}\widetilde{U}_{i,j}) + (\overline{p U_{k,k}} - \overline{p}\widetilde{U}_{k,k}) \\ & + [-\frac{1}{2}\overline{\rho}(\widetilde{U_i U_i U_j} - \widetilde{U_i U_i}\widetilde{U}_j) + \tau_{ij}\widetilde{U}_i + (\overline{\sigma_{ij} U_i} - \overline{\sigma}_{ij}\widetilde{U}_i) - \overline{\rho} R(\widetilde{T U_j} - \widetilde{T}\widetilde{U}_j)]_{,j}. \end{aligned} \tag{19}$$

In practice, two assumptions are introduced to decompose the total SGS dissipation rate into SGS solenoidal part and SGS dilational one. Firstly, assume that the kinematic viscosity ν is spatially uniform over the filter width, so that $\overline{\mu\phi} = \overline{\rho}\nu\tilde{\phi} = \overline{\mu}\tilde{\phi}$. In addition, for compressible turbulence, the assumption $\overline{\sigma}_{ij} = 2\overline{\mu}(\widetilde{S}_{ij} - \delta_{ij}\widetilde{S}_{kk}/3)$ is adopted in previous literature [29,31]. Then, the total SGS dissipation rate ε^{sgs} in Eq. (19) can be rewritten as

$$\begin{aligned} \varepsilon^{sgs} =& \overline{\sigma_{ij} U_{i,j}} - \overline{\sigma}_{ij}\widetilde{U}_{i,j} \\ =& 2\overline{\mu}(\widetilde{S_{ij} U_{i,j}} - \widetilde{S}_{ij}\widetilde{U}_{i,j}) - 2\overline{\mu}(\widetilde{U_{k,k}^2} - \widetilde{U}_{k,k}^2)/3. \end{aligned}$$

Using the fact $S_{ij}S_{ij} = \omega_i\omega_i/2 + U_{i,j}U_{j,i}$, the total dissipation rate ε^{sgs} could be decomposed into SGS solenoidal dissipation rate ε_s^{sgs} and SGS dilational dissipation rate ε_d^{sgs} as follows

$$\begin{aligned} \varepsilon_s^{sgs} =& \overline{\mu}(\widetilde{\omega_i\omega_i} - \widetilde{\omega}_i\widetilde{\omega}_i), \\ \varepsilon_d^{sgs} =& 2\overline{\mu}(\widetilde{U_{i,j} U_{j,i}} - \widetilde{U}_{i,j}\widetilde{U}_{j,i}) - 2\overline{\mu}(\widetilde{U_{k,k}^2} - \widetilde{U}_{k,k}^2)/3, \end{aligned} \tag{20}$$

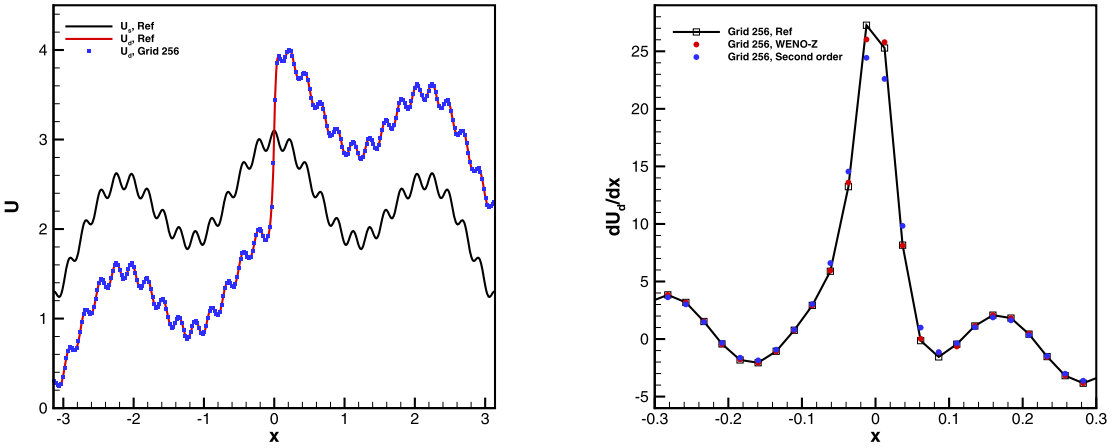

Fig. 12. Initial wave of $U_s(x)$ and $U_d(x)$, and spatial derivative of $U_d(x)$ with the analytical solution, fifth-order WENO-Z reconstruction, and second-order central difference method.

Table 5
Accuracy test of spatial derivative for $U_s(x)$ and $U_d(x)$ with WENO-Z reconstruction.

Waves	$U_s(x)$		$U_d(x)$	
Mesh length	L^2 error	Order	L^2 error	Order
$2\pi/64$	$2.619209e-01$		$3.458353e-01$	
$2\pi/128$	$3.050078e-02$	3.10	$4.959606e-02$	2.81
$2\pi/256$	$3.088122e-03$	4.62	$6.520176e-03$	4.14
$2\pi/512$	$6.699721e-05$	3.98	$4.571909e-04$	3.19

where $\omega_i = \epsilon_{ijk}U_{k,j}$ is the vorticity and $\widetilde{\omega}_i = \epsilon_{ijk}\widetilde{U}_{k,j}$, with the alternating tensor ϵ_{ijk}. With the reasonable assumption $U_{i,j}U_{j,i} \approx U_{k,k}^2$ [21], the SGS dilational dissipation rate ε_d^{sgs} in Eq. (20) can be approximated as

$$\varepsilon_d^{sgs} = 4\overline{\mu}(\widetilde{U_{k,k}^2} - \widetilde{U}_{k,k}^2)/3. \tag{21}$$

The difference between current derivation on dissipation rate in Eq. (20) and Eq. (21), and Eq.(3.4), Eq.(3.5) and Eq.(3.8) in the reference literature [25] should be pointed out. In the reference [25], Eq.(3.4) represents the total dissipation rate instead of the solenoidal dissipation rate.

Appendix C. Consistent spatial derivatives in numerical scheme

The one-dimensional multiple-frequency smooth wave $U_s(x)$ as well as the waves with sharp derivative $U_d(x)$ are used to test the accuracy of spatial derivative. The sharp derivative is designed for simulating the shocklets as shown in Fig. 2. The $U_s(x)$ and $U_d(x)$ are given by

$$\begin{aligned} U_s(x) &= \sum_{i=1}^{3} \alpha_i cos(2\beta_i \pi x), x \in [-\pi, \pi], \\ U_d(x) &= \sum_{i=1}^{3} \alpha_i cos(2\beta_i \pi x) + \tanh(\gamma x), x \in [-\pi, \pi], \end{aligned} \tag{22}$$

where the coefficients $\alpha_1 = 800, \alpha_2 = 80, \alpha_1 = 8$ and $\beta_1 = 0.1, \beta_1 = 0.5, \beta_1 = 2.5, \gamma = 30$ are adopted. Initial waves of $U_s(x)$ and $U_d(x)$ are presented in Fig. 12. Three methods are used to compute the spatial derivative, namely the analytical solution, fifth-order WENO-Z reconstruction [49] and second-order central difference method. Compared with the analytic solution, the fifth-order WENO-Z reconstruction outweighs the second-order central difference method. In current paper, the WENO-Z reconstruction is applied to compute the spatial derivative, which is consistent with the numerical scheme of DNS [8]. The accuracy tests of $U_s(x)$ and $U_d(x)$ with WENO-Z reconstruction are shown in Table 5.

References

[1] Hussein Aluie, Compressible turbulence: the cascade and its locality, Phys. Rev. Lett. 106 (17) (2011) 174502.
[2] Alexei G. Kritsuk, Rick Wagner, Michael L. Norman, Energy cascade and scaling in supersonic isothermal turbulence, J. Fluid Mech. 729 (2013).

[3] Sanjiva K. Lele, Compressibility effects on turbulence, Annu. Rev. Fluid Mech. 26 (1) (1994) 211–254.
[4] A. Hanifi, P.H. Alfredsson, A.V. Johansson, D.S. Hennigson, in: Transition, Turbulence and Combustion Modelling: Lecture Notes from the 2nd ERCOFTAC Summerschool Held in Stockholm, 10–16 June, 1998, vol. 6, Springer Science & Business Media, 2012.
[5] Pierre Sagaut, Claude Cambon, Homogeneous Turbulence Dynamics, vol. 10, Springer, 2008.
[6] Eric Garnier, Nikolaus Adams, Pierre Sagaut, Large Eddy Simulation for Compressible Flows, Springer Science & Business Media, 2009.
[7] G. Kumar, Sharath S. Girimaji, J. Kerimo, Weno-enhanced gas-kinetic scheme for direct simulations of compressible transition and turbulence, J. Comput. Phys. 234 (2013) 499–523.
[8] Guiyu Cao, Liang Pan, Kun Xu, Three dimensional high-order gas-kinetic scheme for supersonic isotropic turbulence I: criterion for direct numerical simulation, Comput. Fluids 192 (2019) 104273.
[9] Jianchun Wang, L-P. Wang, Zuoli Xiao, Y. Shi, S. Chen, A hybrid numerical simulation of isotropic compressible turbulence, J. Comput. Phys. 229 (13) (2010) 5257–5279.
[10] Jianchun Wang, Yipeng Shi, Lian-Ping Wang, Zuoli Xiao, X.T. He, Shiyi Chen, Scaling and statistics in three-dimensional compressible turbulence, Phys. Rev. Lett. 108 (21) (2012) 214505.
[11] Ulrich Schumann, Subgrid scale model for finite difference simulations of turbulent flows in plane channels and annuli, J. Comput. Phys. 18 (1975) 376–404.
[12] Akira Yoshizawa, Kiyosi Horiuti, A statistically-derived subgrid-scale kinetic energy model for the large-eddy simulation of turbulent flows, J. Phys. Soc. Jpn. 54 (8) (1985) 2834–2839.
[13] Siniša Krajnović, Lars Davidson, A mixed one-equation subgrid model for large-eddy simulation, Int. J. Heat Fluid Flow 23 (4) (2002) 413–425.
[14] Giuliano De Stefano, Oleg V. Vasilyev, Daniel E. Goldstein, Localized dynamic kinetic-energy-based models for stochastic coherent adaptive large eddy simulation, Phys. Fluids 20 (4) (2008) 045102.
[15] Sutanu Sarkar, Gordon Erlebacher, M. Yousuff Hussaini, Heinz Otto Kreiss, The analysis and modelling of dilatational terms in compressible turbulence, J. Fluid Mech. 227 (1991) 473–493.
[16] Otto Zeman, On the decay of compressible isotropic turbulence, Phys. Fluids A, Fluid Dyn. 3 (5) (1991) 951–955.
[17] S. Sarkar, The pressure–dilatation correlation in compressible flows, Phys. Fluids A, Fluid Dyn. 4 (12) (1992) 2674–2682.
[18] David C. Wilcox, Dilatation-dissipation corrections for advanced turbulence models, AIAA J. 30 (11) (1992) 2639–2646.
[19] A.M. El Baz, B.E. Launder, Second-moment modelling of compressible mixing layers, in: Engineering Turbulence Modelling and Experiments, Elsevier, 1993, pp. 63–72.
[20] J.R. Ristorcelli, A pseudo-sound constitutive relationship for the dilatational covariances in compressible turbulence, J. Fluid Mech. 347 (1997) 37–70.
[21] David C. Wilcox, et al., Turbulence Modeling for CFD, vol. 2, DCW Industries La Canada, CA, 1998.
[22] Akira Yoshizawa, Statistical theory for compressible turbulent shear flows, with the application to subgrid modeling, Phys. Fluids 29 (7) (1986) 2152–2164.
[23] Eric Pomraning, Christopher J. Rutland, Dynamic one-equation nonviscosity large-eddy simulation model, AIAA J. 40 (4) (2002) 689–701.
[24] Noma Park, Krishnan Mahesh, Numerical and modeling issues in les of compressible turbulence on unstructured grids, in: 45th AIAA Aerospace Sciences Meeting and Exhibit, 2007, p. 722.
[25] Xiaochuan Chai, Krishnan Mahesh, Dynamic-equation model for large-eddy simulation of compressible flows, J. Fluid Mech. 699 (2012) 385–413.
[26] Jeffrey Slotnick, Abdollah Khodadoust, Juan Alonso, David Darmofal, William Gropp, Elizabeth Lurie, Dimitri Mavriplis, Cfd Vision 2030 Study: A Path to Revolutionary Computational Aerosciences, 2014.
[27] Joseph Smagorinsky, General circulation experiments with the primitive equations: I. The basic experiment, Mon. Weather Rev. 91 (3) (1963) 99–164.
[28] Massimo Germano, Ugo Piomelli, Parviz Moin, William H. Cabot, A dynamic subgrid-scale eddy viscosity model, Phys. Fluids A, Fluid Dyn. 3 (7) (1991) 1760–1765.
[29] Bert Vreman, Bernard Geurts, Hans Kuerten, A priori tests of large eddy simulation of the compressible plane mixing layer, J. Eng. Math. 29 (4) (1995) 299–327.
[30] Albertus Willem Vreman, Direct and Large-Eddy Simulation of the Compressible Turbulent Mixing Layer, Universiteit Twente, 1995.
[31] M. Pino Martin, Ugo Piomelli, Graham V. Candler, Subgrid-scale models for compressible large-eddy simulations, Theor. Comput. Fluid Dyn. 13 (5) (2000) 361–376.
[32] Jianchun Wang, Minping Wan, Song Chen, Shiyi Chen, Kinetic energy transfer in compressible isotropic turbulence, J. Fluid Mech. 841 (2018) 581–613.
[33] Prabhu Lal Bhatnagar, Eugene P. Gross, Max Krook, A model for collision processes in gases. I. Small amplitude processes in charged and neutral one-component systems, Phys. Rev. 94 (3) (1954) 511.
[34] Sydney Chapman, T.G. Cowling, The mathematical theory of non-uniform gases: an account of the kinetic theory of viscosity, thermal conduction and diffusion in gases, in: Cambridge Mathematical Library, vol. 1, Cambridge University Press, 1970, pp. 27–52.
[35] Kun Xu, A gas-kinetic bgk scheme for the Navier–Stokes equations and its connection with artificial dissipation and Godunov method, J. Comput. Phys. 171 (1) (2001) 289–335.
[36] Kun Xu, Direct Modeling for Computational Fluid Dynamics: Construction and Application of Unified Gas-Kinetic Schemes, World Scientific, 2015.
[37] Guiyu Cao, Hualin Liu, Kun Xu, Physical modeling and numerical studies of three-dimensional non-equilibrium multi-temperature flows, Phys. Fluids 30 (12) (2018) 126104.
[38] Jiequan Li, Zhifang Du, A two-stage fourth order time-accurate discretization for Lax–Wendroff type flow solvers I. Hyperbolic conservation laws, SIAM J. Sci. Comput. 38 (5) (2016) A3046–A3069.
[39] Liang Pan, Kun Xu, Qibing Li, Jiequan Li, An efficient and accurate two-stage fourth-order gas-kinetic scheme for the Euler and Navier–Stokes equations, J. Comput. Phys. 326 (2016) 197–221.
[40] Liang Pan, Kun Xu, Two-stage fourth-order gas-kinetic scheme for three-dimensional Euler and Navier-Stokes solutions, Int. J. Comput. Fluid Dyn. 32 (10) (2018) 395–411.
[41] Xing Ji, Fengxiang Zhao, Wei Shyy, Kun Xu, A family of high-order gas-kinetic schemes and its comparison with Riemann solver based high-order methods, J. Comput. Phys. 356 (2018) 150–173.
[42] Fengxiang Zhao, Xing Ji, Wei Shyy, Kun Xu, Compact higher-order gas-kinetic schemes with spectral-like resolution for compressible flow simulations, Adv. Aerodyn. 1 (1) (2019) 13.
[43] Shuang Tan, Qibing Li, Zhixiang Xiao, Song Fu, Gas kinetic scheme for turbulence simulation, Aerosp. Sci. Technol. 78 (2018) 214–227.
[44] Guiyu Cao, Hongmin Su, Jinxiu Xu, Kun Xu, Implicit high-order gas kinetic scheme for turbulence simulation, Aerosp. Sci. Technol. 92 (2019) 958–971.
[45] Ravi Samtaney, I. Dale Pullin, Branko Kosović, Direct numerical simulation of decaying compressible turbulence and shocklet statistics, Phys. Fluids 13 (5) (2001) 1415–1430.
[46] Passot Thierry, Annick Pouquet, Numerical simulation of compressible homogeneous flows in the turbulent regime, J. Fluid Mech. 181 (1987) 441–466.
[47] Stephen B. Pope, Turbulent Flows, 2001.
[48] Vinayak Eswaran, Stephen B. Pope, An examination of forcing in direct numerical simulations of turbulence, Comput. Fluids 16 (3) (1988) 257–278.
[49] Marcos Castro, Bruno Costa, Wai Sun Don, High order weighted essentially non-oscillatory weno-z schemes for hyperbolic conservation laws, J. Comput. Phys. 230 (5) (2011) 1766–1792.

[50] Ugo Piomelli, William H. Cabot, Parviz Moin, Sangsan Lee, Subgrid-scale backscatter in turbulent and transitional flows, Phys. Fluids A, Fluid Dyn. 3 (7) (1991) 1766–1771.
[51] Bert Vreman, Bernard Geurts, Hans Kuerten, Realizability conditions for the turbulent stress tensor in large-eddy simulation, J. Fluid Mech. 278 (1994) 351–362.
[52] Alexandre Favre, Equations des gaz turbulents compressibles, J. Méc. 4 (3) (1965).
[53] Leslie SG Kovasznay, Turbulence in supersonic flow, J. Aeronaut. Sci. 20 (10) (1953) 657–674.
[54] Parviz Moin, Kyle Squires, W. Cabot, Sangsan Lee, A dynamic subgrid-scale model for compressible turbulence and scalar transport, Phys. Fluids A, Fluid Dyn. 3 (11) (1991) 2746–2757.
[55] Solomon Kullback, Richard A. Leibler, On information and sufficiency, Ann. Math. Stat. 22 (1) (1951) 79–86.